Mode I Traction-Separation Measured Using Rigid Double Cantilever Beam Applied to Structural Adhesive

B Watson[1], CH Liao[1], MJ Worswick[1], DS Cronin[1]

[1]Department of Mechanical and Mechatronics Engineering, University of Waterloo,

Acknowledgements: The authors would like to express their thanks to Honda Research and Development Americas, 3M Canada Company, ArcelorMittal, Compute Canada and the Natural Sciences and Engineering Research Council of Canada (NSERC) for their support of this research.

Abstract

Adhesive joining facilitates the development of multi-material vehicle structures; however, widespread adoption requires material properties to characterize adhesive joints for implementation in finite element (FE) models. Specifically, modeling adhesive joints using the cohesive zone method requires measuring the Mode I traction-separation response, which currently requires multiple tests. To address this need, a new method to determine the Mode I response was developed using the Rigid Double Cantilever Beam (RDCB) test, where the steel adherend geometry was designed to ensure high stiffness compared to structural epoxy adhesives. The samples were tested in tension with displacements measured from high-resolution imaging of the test. A new analysis method was developed with resulting Mode I traction-separation response within the expected range for this structural adhesive. The analysis was verified using a FE model of the test and compared to Tapered Double Cantilever Beam test data. Importantly, the predicted force-displacement response from the FE model, using the measured traction-separation curve, compared well to the measured force-displacement data. The

proposed RDCB test demonstrated the ability to determine the Mode I response of a toughened structural adhesive using a single test, the results of which can then be readily implemented into FE simulations.

Keywords: Mode I, structural adhesive, cohesive zone modeling, traction-separation curve

Nomenclature

b = length of the bond line

B = sample thickness

$E_{adherend}$ = Young's modulus of adherend

F = applied force on loading pins

L = distance from the edge of the sample to the point of loading

S_{init} = initial slope of traction-separation response

t(x), t(δ) = arbitrary traction–displacement functions

t_c = peak compression traction

v = length on axis perpendicular to bond line with origin at center of bond line

x = length on axis parallel to bond line with origin at $\mu = 0$

α = rigidity ratio

δ = crack opening (separation)

δ_c = closing distance at the edge of the sample due to the compression of the bond line

Δ = load point opening displacement

$\upsilon_{adherend}$ = Poisson's ratio of adherend

μ = distance from edge of sample to transition between tensile and compressive loading of bond line

1 Introduction

The need to improve fuel economy by reducing vehicle mass has led designers to explore multi-material lightweight structures [1]; however, traditional joining methods may lead to new complications when used to join dissimilar materials (*e.g.* galvanic corrosion and residual thermal stresses when joining steel and aluminum). Multi-material joining challenges may be addressed in part using structural adhesives [2]; however, the ability to model the response of structural adhesive joints in crash scenarios is essential to enable design with adhesives and further widen their implementation in modern production vehicles.

The cohesive zone method (CZM) is often used to model adhesive joints since it is computationally efficient while providing an accurate representation of the material properties in Model I (opening, or tension) and Mode II (shear) [3]. When this technique is used to model adhesive joints, a single row of elements is generally defined between adherends to define the bond line. The CZM model assumes that damage accumulates within the material ahead of the extending crack tip, along a predefined path [4], eventually leading to failure along the pre-defined path. Unlike traditional material constitutive models, which require a relationship between stress and strain, cohesive zone models use traction-separation (stress-displacement) descriptions in the normal (Mode I) and shear (Mode II) directions to describe the material response [5; 6]. The traction-separation curves, often having a triangular or trapezoidal law (Figure 1), are defined using the undamaged material stiffness, peak traction and critical energy release rate (the area under the traction-separation curve). A trapezoidal traction-separation

definition also requires specification of the amount of plastic deformation relative to the total deformation [7].

The Mode I fracture energy, the energy per unit area required to create a new surface, is often measured using the double cantilever beam (DCB) test comprised of two bonded beams [8] which are pulled apart until a crack propagates in the adhesive. The elastic energy stored in the beams is converted to energy used to create a free surface once crack initiation proceeds. The critical energy release rate can be calculated by using the Irwin-Kies equation [9] (e.g. ASTM D3433 [10], ISO 25217 [11]). However, the change in compliance relative to crack length, an important term in the Irwin-Kies equation, cannot be directly measured leading to several different methods being proposed to estimate the change in compliance and, thus, measure critical energy release rate. Lopes *et al.* [12] compared three analysis techniques using DCB samples and three analysis techniques using tapered double cantilever beam (TDCB) samples, in which the sample geometry is designed to have a constant compliance irrespective of crack length [13]. The authors identified that for toughened adhesives, the critical energy release rate calculated from DCB testing was higher than that measured using TDCB samples, especially when comparing DCB results using the compliance beam bending method (CBBM) analysis technique [14] to the comparatively simple beam theory TDCB analysis technique suggested in ASTM D3433 [10] and concluded that TDCB analysis techniques are not suited to measure critical energy release rates outside of conditions under which linear elastic fracture mechanics can be used. While DCB or TDCB tests can provide a measure of the fracture energy in Mode I, additional data are required to describe the traction-separation response such as tensile testing of butt-joints to measure peak traction [15] and initial stiffness. Additionally, the high mass of DCB

and TDCB specimens can potentially introduce larger inertial effects when loading at elevated velocity.

To address challenges with traditional DCB or TDCB test samples, a rigid double cantilever beam (RDCB) geometry was proposed [16] to measure the traction-separation response in a single test for proteinaceous adhesives. This analysis technique was later refined for use with structural adhesives [17]. In the latter study, the adherend geometry was selected such that the second moment of area in the bending direction was very large (Figure 2a). Additionally, the steel adherend stiffness was two orders of magnitude higher than the adhesive, so the assumption of rigid adherends was satisfactory. The loading (Figure 2b) was assumed to produce rigid body rotation of the adherends about the end of the sample far away from the load point (orange dot in Figure 2), implying that the entire bond length was subjected to tensile loading (Figure 2c). Using a moment equilibrium balance, the authors demonstrated that the response of an adhesive could be determined from the load point opening displacement and force measurement. This analysis technique, under quasi-static loading (3 mm/min), was then used to characterize the peak traction (σ_m) and critical energy release rate (G_{IC}) for three adhesives: a soft silicone-based elastomer (σ_m = 1 MPa, G_{IC} = 100 J/m^2); a polyurethane-based adhesive (σ_m = 6 MPa, G_{IC} = 430 J/m^2); and, an un-toughened epoxy (σ_m = 9 MPa, G_{IC} = 70 J/m^2). The authors noted that, in toughened epoxy tests, the use of DCB samples resulted in peak stress values of 14 MPa and critical energy release rates of 700 J/m^2 [18], which were both considerably higher than those measured using the RDCB geometry. Liao *et al.* [19] used the RDCB analysis technique to extract the traction-separation response of a toughened epoxy and measured a peak traction of 35 MPa and critical energy release rate of 3400 J/m^2. Other authors have measured values of 35.8 MPa and 3607 J/m^2 [15] and 100 MPa and 1400 J/m^2 [20], though these values are highly

dependent on the specific adhesive being tested, bond line thickness [21, 22], and loading rate [15].

In the current study, a new analysis of the RDCB test sample was developed to include a compressive region within the adhesive bond line. This enhanced analysis allowed for the full traction–separation response of a structural adhesive to be determined from a single test, rather than the need to perform multiple tests or to use inverse methods to extract the necessary material parameters.

2 Experimental and Numerical Methodology

The Mode I properties of a structural adhesive (3M Impact Resistant Structural Adhesive 7333, 3M Canada Company, London, Ontario) were measured using a proposed RDCB geometry and newly introduced analysis. The measured traction-separation curves were then used in FE models to verify the analysis method by comparing the measured and model force-displacement response, and to quantitatively assess the assumption of rigid adherends. For comparison to an existing methodology, ASTM D3433 TDCB experimental tests were undertaken with the structural adhesive. Finally, a model of the ASTM D3433 TDCB test was created using cohesive parameters measured using the new RDCB analysis technique and compared to experimental results from the TDCB tests, highlighting the interchangeability of the new technique with a commonly accepted test to assess the Mode I response of structural adhesives. It is important to note that throughout this study, FE modeling has only been used to demonstrate the ability of the new analysis technique to extract a full traction-separation response experimentally, meaning no inverse modeling has been used for parameter extraction.

2.1 RDCB Sample Preparation and Testing

The dimensions of the adherends used in this study (Figure 3) were determined to minimize the mass of the sample, for future dynamic testing, while maximizing the bending stiffness. In the original analysis, Dastjerdi *et al.* provided a measure to estimate the rigidity of the adherend (α, Equation (1) [17]) based on the elastic properties of the adherend ($E_{adherend}$ and $\upsilon_{\text{adherend}}$) and the expected undamaged stiffness of the adhesive traction-separation response (S_{init}). A value of α=1.0 indicated a perfectly rigid adherend. The sample dimensions used in this study (Figure 3) had a corresponding α parameter of 0.932, indicating a high stiffness of the adherends, relative to the adhesive. The adherends were machined from 6.2 mm thick 1008 steel with a yield strength of 345 MPa and a Young's modulus of 207 GPa.

$$\alpha = \left(1 + \frac{Bb^3 S_{init} \left((1+\upsilon_{adherend}) \frac{2}{Bh} \left(\frac{9}{5} L \left(\frac{L}{b} - 1 \right) \right) + \frac{12}{Bh^3} \left(\frac{L^3}{3} + \frac{Lb^2}{10} - \frac{2L^2 b}{5} \right) \right)}{3L^2 E_{adherend}} \right)^{-1} \quad (1)$$

The bond surfaces of the samples were grit blasted with 60 grit silicon carbide abrasive media for 10 s each at a pressure of 480 kPa and cleaned with methyl-ethyl ketone (MEK) immediately prior to bonding to remove contamination from the metal surfaces. Early testing in which grit blasting was not performed led to high variability and low average strength due to interfacial failure. The grit blasted samples reported in the current study exhibited cohesive failure.

A portion of the bond line was masked using correction tape (Pilot Begreen Whiteline RT) to prevent the adhesive from bonding to locations outside the desired bond area, leaving 13.25 mm of exposed surface (dimension *b* in Figure 3) to apply the two-part toughened epoxy to each of the adherends. The adherends were brought together and were placed in a custom-made fixture (Figure 4) for curing with shims inserted between the adherends in the unbonded portion of the sample to control the bond line thickness (0.64 mm average) and length (13.2 mm average). The

shim was also used to provide a consistent notch at the leading edge of the adhesive bond line, though no pre-fatiguing was carried out to develop a sharp crack tip. Due to the high toughness of the material tested, the results were not sensitive to the initial notch; however, testing more brittle materials with this methodology may require pre-cracking. This fixture was developed over several iterations to produce samples with good alignment of the adherends. The fixture was designed to ensure the adherends lay in the same plane. A groove was machined in the area underneath the bond line to provide space for excess adhesive to flow after the two adherends were located in the fixture.

The samples were cured according to the manufacturers specifications (30 min. after reaching 80 ^{o}C, measured using a thermocouple attached to the sample) using a forced convection oven (Binder ED-53). After curing, excess adhesive was removed to ensure the bond line was flush with the adherends on all sides. The bond line length and thickness of each sample were then measured using an opto-digital microscope (VHX 5000, Keyence), which could resolve these measurements to 10 μm accuracy.

A total of 9 test repeats were carried out using an Instron Model 4465-Standard test machine with a 5 kN capacity load cell. The cross-head speed was 0.0115 mm/s, corresponding to the lowest cross-head speed available for this test frame. In addition to the force response measured from the load frame, 30 fps video was used to accurately monitor the displacement of the loading pins (Figure 5) using a 105 mm macro lens and digital single-lens reflex (DSLR) camera (Nikon 3200; 1920 x 1080 pixels, approximately 30 pixels/mm). The use of optical methods to measure displacement when testing strong adhesive bonds has been shown to be a better measure of the displacement than a machine-mounted displacement transducer [23] since the crosshead displacement measurement includes compliance in the test machine and grips. Deformation from

this additional compliance is often on the same order of magnitude as the displacement-to-failure of the bond line. Additionally, the necessity to fix an LVDT or crack opening displacement gauge to the specimen would add additional mass to the sample, which could introduce undesirable inertial effects when adapting the specimen to high rate loading. The displacement of the pins was tracked using the imaging tracking software [24].

2.2 RDCB Sample Analysis and Traction-Separation Curve

A previous analysis of the RDCB by Dastjerdi *et al.* [16] assumed a center of rotation on the left boundary of the sample (Figure 2). In contrast, FE analysis of the sample during the preliminary portion of this study revealed that a portion of the bond line was in compression. Thus, the analysis of Dastjerdi *et al.* [16] was extended such that the center of rotation was defined as a point located a distance μ from the edge of the sample furthest from the loading location (Figure 5c). Note that while a linear tensile force distribution is shown to simplify the explanation that follows, the response will not generally be linear under tensile loading.

Using the assumption that the adherends remain rigid, three displacement measures of interest can be related by:

$$\frac{\delta_c}{\mu} = \frac{\delta}{b-\mu} = \frac{\Delta}{L-\mu} \tag{2}$$

In the present study, L was 22.23 mm. Similarly, the displacement v, transverse to the bond line, at any point along the bond line length x (using the coordinate system shown in Figure 5) can be defined by:

$$\mathrm{v}(x) = \frac{\delta}{b-\mu} x = \frac{\Delta}{L-\mu} x \tag{3}$$

In general, a CZM assumes that the material does not experience yielding or damage in Mode I compression and symmetry of the compression-tension stiffness response is often assumed, as

demonstrated experimentally by Adams and Coppendale [25] for an epoxy system. By using these assumptions, the peak compression traction, can be defined by:

$$t_c = \frac{S_{init}\mu\Delta}{L-\mu} \tag{4}$$

For adhesive systems where these assumptions cannot be assumed, further refinement of the compression response would need to be carried out. A sum of forces in the vertical direction based on the free body diagram (Figure 5), yields:

$$F + \frac{1}{2}\mu B t_c = B\int_0^{b-\mu} t(x)dx \tag{5}$$

Similarly, a moment balance about the point of rotation ($x = 0$) can be expressed as:

$$F(L-\mu) - \frac{2}{3}\mu\frac{1}{2}\mu B t_c = B\int_0^{b-\mu} xt(x)dx \tag{6}$$

Note that Equation (5) and Equation (6) allow for an arbitrary shape of the traction-separation response to be assumed, however, the initial tensile response of most traction-separation cohesive laws are treated as linear up to the point of peak traction and the initial stiffness (S_{int}) must be calculated. Within this linear region, the integral in the force balance (Equation (5)) becomes:

$$\int_0^{b-\mu} t(x)dx = \frac{1}{2}t_o(b-\mu) \tag{7}$$

Similarly, for the moment balance (Equation (6)):

$$\int_0^{b-\mu} xt(x)dx = \frac{1}{3}t_o(b-\mu)^2 \tag{8}$$

Also in the linear region, the peak traction in the compression zone can be expressed as:

$$t_c = \frac{\mu t_o}{b-\mu} \tag{9}$$

By substituting Equation (7) through Equation (9) into Equation (5) and Equation (6), rearranging these equations to isolate the force, then equating the resulting two expressions and solving for μ:

$$\mu_{elastic} = \frac{3Lb-2b^2}{6L-3b} \tag{10}$$

Note that this expression is only valid in the initial linear elastic region. In a similar manner, by substituting Equation (4), Equation (7), and Equation (8) into Equation (5) and Equation (6), the initial stiffness (S_{init}), as a function of the initial slope of the force-displacement response (F/Δ) can be expressed as:

$$S_{init} = \frac{F}{\Delta}\left(\frac{2(b-\mu_{elastic})(L-\mu_{elastic})}{B{\mu_{elastic}}^2}\right)\left(\left(\frac{(b-\mu_{elastic})}{2} - \frac{{\mu_{elastic}}^2}{2(b-\mu_{elastic})}\right)^{-1} - (b-\mu_{elastic})^{-1}\right) \tag{11}$$

In order to convert the traction-separation responses from being functions of position along the bond line length to functions of adherend separation, a change of variable substitution using Equation (3) to relate x to v was performed on Equation (5), leading to:

$$\frac{F}{B} + \frac{\mu^2 S_{init}\Delta}{2(L-\mu)} = \frac{L-\mu}{\Delta}\int_0^\delta t(v)dv \tag{12}$$

Differentiating Equation (12) with respect to δ and simplifying leads to the following expression for traction-separation:

$$\frac{d\Delta}{d\delta}\frac{d}{d\Delta}\left(\frac{F\Delta}{B(L-\mu)} + \frac{\mu^2 S_{init}\Delta^2}{2(L-\mu)^2}\right) = t(\delta) \tag{13}$$

Similarly, a change of variable in the moment balance can be expressed as:

$$\frac{F(L-\mu)}{B} - \frac{\mu^3 S_{init}\Delta}{3(L-\mu)} = \left(\frac{L-\mu}{\Delta}\right)^2\int_0^\delta vt(v)dv \tag{14}$$

Which can then be expressed as:

$$\frac{(L-\mu)}{\Delta(b-\mu)}\frac{d\Delta}{d\delta}\frac{d}{d\Delta}\left(\frac{F\Delta^2}{B(L-\mu)}-\frac{\mu^3 S_{init}\Delta^3}{3(L-\mu)^3}\right)=t(\delta) \quad (15)$$

Equating Equation (13) and Equation (15), leads to:

$$\frac{d\Delta}{d\delta}\frac{d}{d\Delta}\left(\frac{F\Delta}{B(L-\mu)}+\frac{\mu^2 S_{init}\Delta^2}{2(L-\mu)^2}\right)=\frac{(L-\mu)}{\Delta(b-\mu)}\frac{d\Delta}{d\delta}\frac{d}{d\Delta}\left(\frac{F\Delta^2}{B(L-\mu)}-\frac{\mu^3 S_{init}\Delta^3}{3(L-\mu)^3}\right) \quad (16)$$

Of the variables in Equation (16), only μ is unknown. To solve for μ as a function of Δ, a script was written in which both sides of Equation (16) were evaluated for 1,000 equally spaced values of μ between $\mu_{elastic}$ and 0 for each increment of displacement in the force-displacement response from the experiments. The value of μ, which provided the minimum difference between the two sides of Equation (16), was then selected as the value of μ for a given load point opening displacement. Concurrent to this calculation for each load point opening displacement increment, the crack opening was calculated using Equation (2) and the traction was calculated using Equation (13) and Equation (15), ensuring the two traction calculations provided the same response as a check of the analysis. This script then provided the traction-separation curve for a given experimentally measured force-displacement.

2.3 RDCB Finite Element Model

To assess the analytical model presented in the previous section of this paper and demonstrate the ability of the cohesive parameters extracted during testing to reproduce the measured force and opening displacement response, two three-dimensional finite element (FE) models of the RDCB tests (Figure 6) were created using the commercial FE code, LS-Dyna V7.1.2 MPP [26]; one model used rigid adherends and one model used deformable adherends. Models of each of the 9 test repeats were created using sample-specific traction-separation responses and bond line dimensions. Detailed geometry of the adherends was generated using 0.5 mm linear hexahedral elements with selectively reduced integration. A mesh sensitivity study was carried out by

rerunning the model with each element split into 8 hexahedral elements, which produced identical results to the nominal mesh. The deformable models, created to assess the rigidity assumption, used an elastic constitutive material model for the steel adherends with density of 7800 kg/m^3, Young's modulus of 207 GPa and Poisson's ratio of 0.3. In both the deformable and rigid analyses, the pins (also meshed with nominal 0.5 mm cubic hexahedral elements) were assigned rigid material properties with contact defined between the pins and adherends. The lower pin was fixed in all directions, while a prescribed velocity was applied in the vertical direction to the top pin with motion in all other directions being fixed, as was the case in the experiment. A layer of cohesive elements was defined between the adherends to simulate the bond line of the joint, with the bond line length corresponding to that measured on each of the 9 samples prior to testing. A cohesive material definition (*MAT_240 in LS-DYNA), based on the properties measured from each test repeat, was then applied to the model of each individual test. The Mode II response was determined from shear testing using a methodology similar to that presented by Trimino and Cronin [3] in which thick adherend lap shear testing was carried out with a 1 mm thick bond-line to measure the traction-shear strain response of the adhesive. The separation response was then calculated based on strain response and the bond line thickness for the test sample of interest. Since the loading was purely in Mode I, the Mode II response did not affect the outcome of the simulation, but was required for a complete definition of the cohesive model.

2.4 TDCB Testing and Finite Element Model

As an independent assessment of the accuracy of the analysis in extracting the Mode I cohesive properties of the adhesive, TDCB testing was carried out using the ASTM D3433 standard sample [10]. The test samples (Figure 7a) were machined from A36 steel and were grit blasted

and cleaned with MEK immediately prior to bonding. Shim stock was used to create a bond line thickness similar to the average measured from the RDCB samples (RDCB average = 0.64 mm, TDCB average = 0.653 mm). A total of four samples were loaded at a constant rate (0.015 mm/s) to failure, with the load point opening displacement tracked from the test video determined as a function of applied force recorded for each test. A model of this TDCB test was then created (Figure 7b) using the same methodology as adopted for the RDCB deformable models, described above, with averaged cohesive material properties from the RDCB experiments. The results of the TDCB tests were then compared to the model response using the cohesive traction-separation derived from RDCB testing to assess, independently, the ability of the proposed RDCB test and analysis to represent the material response in Mode I loading.

3 Results and Discussion

3.1 RDCB Experiments

The experimental data (Figure 8) showed good repeatability with an average measured peak force of 592 N (standard deviation 45 N). The peak force occurred at an average load point opening displacement of 0.125 mm (standard deviation 0.02 mm). Note that each test was arrested after the crack began to advance along the bond line and all the necessary data needed to create traction–separation response had been collected. The point on each experimental force-displacement response corresponding to the end of the traction-separation response has been marked with a red ‘X’ to indicate the crack propagation.

Although tracking of the propagating crack tip was possible, previous testing demonstrated that a large amount of magnification was required to monitor the crack and a high signal-to-noise ratio was present so that the measurements were not consistent. However, the measurement of pin displacement enabled a direct measure of test sample deformation that did not include

compliance of the test apparatus, while providing consistent displacement measurements using standard camera lenses and conventional teleconverters, which could also be mounted on high speed cameras in future high rate testing. While the pixel density used to measure the pin displacement was relatively coarse for this series of tests, the repeatability, given the small displacements being measured, indicate that this resolution was acceptable. A higher pixel density could be used to further refine the displacement measurement.

Applying the analysis described above, the force-displacement response was converted to a traction-separation curve. Based on the shape of the resulting curves, a trapezoidal cohesive law [27 - 29] was selected as an appropriate representation of the test response to be used in a cohesive zone model (example shown in Figure 9). This shape was selected due to the ability of this simplified response to provide a good fit to the experimental data and the availability of this cohesive zone law in the LS-DYNA FE code, although a more generic traction-separation response (one defined by a set of data points, for example) could also be used, if needed, to further enhance the representation of the material behavior. The least squares fit used in this study did not preclude the use of a triangular traction-separation law, which can be viewed as a special case of a trapezoidal law with zero area under the plastic portion of the response. The relatively small plastic portion of the response for the adhesive tested indicates that while a trapezoidal law was found to be the optimal response, a triangular law would provide a reasonable approximation of the response.

A least squares approach was used to fit the trapezoidal traction-separation response to the data from each test, in which the peak traction, critical energy release rate (the area under the traction-separation response), and the ratio of the area under the flat portion of the response to the total

response were optimized to minimize the error between the test response and the fit. Note that the slope of the initial linear region was previously determined using Equation (11).

The resulting test sample and material parameters (Table 1) were used in the test sample-specific FE models, while the average data was used for the TDCB simulations.

3.2 Finite Element Analysis of RDCB Test Sample

During the initial loading of the sample, the traction along the bond line increased most rapidly at the crack tip (Figure 10, stage 1) and created a linear stress gradient along the bond line length (Figure 10, stage 2) until the traction at the crack tip reached the peak stress of the trapezoidal traction-separation response. The length of the compressive zone (shown in grey in Figure 10), corresponding to the $\mu_{elastic}$ distance calculated based on the updated test analysis, validated the stress distribution used in the current analysis. As loading continued, more of the bond line reached the stress plateau (Figure 10, stage 3) until the material at the crack opening began to experience damage (corresponding to the decrease in traction). Finally, the elements closest to the loading point reached zero stress (Figure 10, stage 4), before being eroded, initiating the crack advancing along the bond line (Figure 10, stage 5). It is also apparent that the zone of compression became smaller (*i.e.* μ decreased) as the material began to undergo damage.

The FE models with rigid and deformable adherends were able to reproduce the force-displacement response of the individual tests in all cases. For example, when comparing the rigid and deformable model responses to the force-displacement measured from Test 8 (Figure 11), R^2 values of 0.999 and 0.991, respectively, were obtained. The initial slope of the deformable model was, on average, 10% lower than the rigid model. This indicated that the rigidity assumption of the adherends was reasonable for the geometry and adhesive used in this study.

A comparison of the shift in the neutral axis (*i.e.* length of μ as measured from the edge of the sample (Figure 5) as a function of the load point opening displacement response calculated from the test data using Equation (16) and that predicted by the rigid FE model (Figure 12) showed excellent agreement (R^2 = 0.998). One interesting aspect to these responses is the significant level of oscillation early in the response due to the calculations using expressions with ratios of very small displacements. In reality, μ should be constant until the onset of the plastic region of the response (*i.e.* between 0.0 mm and 0.075 mm load point opening displacement in Figure 12).

Using the original analysis presented by Dastjerdi *et al.* [16, 17] to extract a traction-separation from a known input resulted in the model underpredicting the peak traction by 15%. This result was due to the tensile traction not counteracting the portion of the bond line in compression, leading to a lower calculated peak traction value. Consequently, a check on the interrelationship between the traction-separation and force-displacement failed using the original analysis.

A so-called “average cohesive model”, using the mean test response for each material parameter, was integrated into a rigid FE model with a bond line length equal to the average of that measured prior to testing (13.20 mm). The response of this model, when compared to the test responses (Figure 13), was shown to provide a representative response of both the traction-separation of the tested samples, and the force-displacement response with a peak force of 593 N (compared to 592 N measured average) occurring at a load point opening separation of 0.127 mm (*versus* 0.125 mm measured average).

While the Mode II traction-separation response was kept constant for all simulations performed in this work, a small study was carried out to ensure that the Mode II response had no effect on the model output, which was confirmed. This study also, indirectly, indicates that the mode mixity response was not relevant for the current analysis.

3.3 TDCB Finite Element Model using Traction-Separation Curve from RDCB Tests

Testing of the same structural adhesive was also carried out using the standard ASTM D3433 TDCB test geometry to ensure the new analysis technique provided results which would be comparable to those provided by a widely accepted test specification [12; 30]. Note that for this testing the samples were loaded monotonically to an unstable failure, unlike the practice suggested in the ASTM D3433, in which the sample is loaded and unloaded to test both crack propagation and crack arrest energy release rates. Analyzing the results using the recommended method in the ASTM D3433 standard, the average critical energy release rate (2.552 kJ/m^2) was considerably lower (19.7%) than that measured using the RDCB analysis (3.055 kJ/m^2). This lower G_{IC} value is consistent with a comparison between TDCD and DCB samples carried out by Lopes *et al.* [12] in which TDCB testing of a ductile epoxy (Araldite 2015) and a ductile polyurethane (Sikaforce 7752) produced lower (30.1% and 36.4%, respectively) G_{IC} values than using DCB samples.

Given the difference between calculated G_{IC} values for TDCB and DCB or RDCB tests, the traction-separation curves determined using the proposed analysis method were applied to a model of the TDCB, and the predicted force-displacement results were compared with the measured data (Figure 14). The force-displacement response from the physical tests was in good agreement with the TDCB model using the adhesive properties from the RDCB analysis (average R^2 value of 0.917). The predicted ultimate failure is also in good agreement with an average failure displacement of 4.2 mm in the experiment and a predicted failure displacement of 4.3 mm in the TDCB model. While the peak forces were in good agreement between the test average (4815 N) and the model (4934 N), the force required to initiate damage was lower in the tests than predicted by the model. The model exhibited the expected constant force measurement

as the crack extended. Blackman *et al.* [31] has suggested the increase in force as the crack extends along the length of the bond line was due to an increase in compliance of the TDCB sample stemming from the discontinuous TDCB profile (*i.e.* the location of the crack tip in the sample used in this study) and the need to correct for rotation of the adherend at the root of the crack tip opening. Similar comparisons between experimental and simulated responses were shown by Karac *et al.* [32] and Alvarez *et al.* [33] who modeled DCB.

Further refinement of the compression response of the adhesive bond may potentially provide improvements to the overall response of the analysis, though the ability of the current methodology to capture the TDCB test response reasonably well suggests that this would likely only provide a minor improvement to the analysis.

4 Conclusions

The primary advantage of the proposed test sample and analysis, which considered the compression region in the bond line during loading, was the ability to extract the entire Mode I traction-separation response using a single test. With careful fixturing during curing and proper surface preparation, the RDCB sample was straightforward to test and demonstrated good repeatability.

The measured traction-separation curves were implemented in test-specific FE simulations, which were shown to reproduce the measured force-displacement response using rigid adherends. The deformable adherend model exhibited a 10% lower initial stiffness compared to the rigid adherends, supporting the assumption that the adherend rigidity used to develop the current analysis technique was acceptable.

Validation of the analysis technique was further undertaken using the ASTM D3433 TDCB test sample geometry with the same bond line thickness as was used in the RDCB test samples. A model of the TDCB sample geometry combined with the cohesive parameters determined from the RDCB test using the new analysis was shown to accurately predict the force-displacement response of an independent series of TDCB tests.

A further advantage of the method proposed in this study is the significantly lower mass of the RDCB sample (~56 g) compared to traditional test samples such as the ASTM D3433 TDCB sample (~2040 g). While elevated rate loading was not investigated in this study, the lower mass of the RDCB sample will reduce inertial effects, enabling Mode I characterization of adhesive joints at high deformation rates.

References

[1] Goede, M. *Sustainable Production Technologies of Emission reduced Lightweight car concepts (SuperLIGHT-CAR): Publishable Final Activity Report*; European Commission Community Reshearch and Development Information Service: Brussles, 2009.

[2] Conklin, J.; Beals, R.; Brown, Z. BIW Design and CAE. *SAE Tech. Pap. Ser*. **2015**, 2015-01-0408. DOI:10.4271/2015-01-0408

[3] Trimino, L.; Cronin, D. Evaluation of Numerical Methods to Model Structural Adhesive Response and Failure in Tension and Shear Loading. *J. of Dynamic Behavior of Materials*. **2016**, *2(1)*, 122-137. DOI: 10.1007/s40870-016-0045-7

[4] da Silva, L.; Campilho, R. *Advances in numerical modelling of adhesive joints*; Springer Berlin: Heidelberg, 2012.

[5] Yang, Q.; Thouless, M. Mixed-mode fracture analyses of plastically-deforming adhesive joints. *Int. J. Fract*. **2001**, *110(2)*, 175-187. DOI: 10.1023/A:1010869706996

[6] Hallquist, J. *LS-DYNA Keyword User's Manual Volume II-R8876*; Livermore Software Technology Corporation: Livermore, 2017.

[7] Marzi, S.; Hesebeck, O.; Brede, M.; Kleiner, F. A rate-dependent, elasto-plastic cohesive zone mixed-mode model for crash analysis of adhesively bonded joints. Presented at the 7th European LS-DYNA conference, Salzburg, Austria, May 14-15, 2009.

[8] Irwin, G.; Kies, J. Critical Energy Rate Analysis of Fracture Strength. *Weld. J., Research Supplement*. **1954**, *33*, 193s-198s.

[9] Ripling, E.; Mostovoy, S.; Patrick, R. Application of fracture mechanics to adhesive joints. In *Adhesion*; ASTM International: Philadephia, 1964; pp 5-16.

[10] ASTM D3433-99. Standard Test Method for Fracture Strength in Cleavage of Adhesives in Bonded Metal Joints, American Society for Testing and Materials 2014.

[11] ISO 25217:2009. Adhesives – Determination of the mode 1 adhesive fracture energy of structural adhesive joints using double cantilever beam and tapered double cantilever beam specimens, International Organization for Standardization. 2009.

[12] Lopes, R.; Campilho, R.; da Silva, F.; Faneco, T. Comparative evaluation of the Double-Cantilever Beam and Tapered Double-Cantilever Beam tests for estimation of the tensile fracture toughness of adhesive joints. *Int. J. Adhes. Adhes*. **2016**, *67*, 103-111. DOI: 10.1016/j.ijadhadh.2015.12.032

[13] Ripling, E.; Mostovoy, S.; Corten, H. Fracture mechanics: a tool for evaluating structural adhesives. *J. Adhes*. **1971**, *3(2)*, 107-123. DOI: 10.1080/00218467108081158

[14] De Moura, M. F. S. F.; Campilho, R. D. S. G.; Gonçalves, J. P. M. Crack equivalent concept applied to the fracture characterization of bonded joints under pure mode I loading.

Composites Sci. Technol. **2008**, *68(10-11)*, 2224-2230. DOI: 10.1016/j.compscitech.2008.04.003

[15] Marzi, S.; Hesebeck, O.; Brede, M.; Kleiner, F. A rate-dependent cohesive zone model for adhesively bonded joints loaded in mode I. *J. Adhes. Sci. Technol*. **2009**, *23(6)*, 881-898. DOI: 10.1163/156856109X411238

[16] Dastjerdi, A.; Pagano, M.; Kaartinen, M.; McKee, M.; Barthelat, F. Cohesive behavior of soft biological adhesives: experiments and modeling. *Acta Biomater*. **2012**, *8(9)*, 3349-3359. DOI: 10.1016/j.actbio.2012.05.005

[17] Dastjerdi, A.; Tan, E.; Barthelat, F. Direct measurement of the cohesive law of adhesives using a rigid double cantilever beam technique. *Exp. Mech*. **2013**, *53(9)*, 1763-1772. DOI: 10.1007/s11340-013-9755-0

[18] Högberg, J.; Sørensen, B.; Stigh, U. Constitutive behaviour of mixed mode loaded adhesive layer. *Int. J. Solids Struct*. **2007**, *44(25)*, 8335-8354. DOI: 10.1016/j.ijsolstr.2007.06.014

[19] Liao, C.-H.; Watson, B.; Worswick, M.; Cronin, D. Mode I RDCB Test and Analysis Incorporating Adhesive Compliance Applied to Structural Adhesives. Presented at the 2017 Conference and Exposition on Experimental and Applied Mechanics, Indianapolis, USA, June 12-15, 2017.

[20] Yang, Q.; Thouless, M.; Ward, S. Numerical simulations of adhesively-bonded beams failing with extensive plastic deformation. *J. Mech. Phys. Solids*. **1999**, *47(6)*, 1337-1353. DOI: 10.1016/S0022-5096(98)00101-X

[21] da Silva, L.; Rodrigues, T.; Figueiredo, M.; De Moura, M.; Chousal, J. Effect of adhesive type and thickness on the lap shear strength. *J. Adhes*. **2006**, *82(11)*, 1091-1115. DOI: 10.1080/00218460600948511

[22] Davies, P.; Sohier, L.; Cognard, J.; Bourmaud, A.; Choqueuse, D.; Rinnert, E.; Créac'hcadec, R. Influence of adhesive bond line thickness on joint strength. *Int. J. Adhes. Adhes*. **2009**, *29(7)*, 724-736. DOI: 10.1016/j.ijadhadh.2009.03.002

[23] da Silva, L.; da Silva, R.; Chousal, J.; Pinto, A. Alternative methods to measure the adhesive shear displacement in the thick adherend shear test. *J. Adhes. Sci. Technol*. **2008**, *22(1)*, 15-29. DOI: 10.1163/156856108X292241

[24] Brown, D.; Christian, W. Simulating what you see: combining computer modeling with video analysis. Presented at the 8th International Conference on Hands on Science, Ljubljana, Slovenia, Oct 11-13, 2011.

[25] Adams, R.; Coppendale, J. The Stress-Strain Behaviour of Axially-Loaded Butt Joints. *J. Adhes*. **1979**, *10(1)*, 49-62. DOI: 10.1080/00218467908544611

[26] Hallquist, J. *LS-DYNA Theory Manual-R8697*; Livermore Software Technology Corporation: Livermore, 2017.

[27] Tvergaard, V.; Hutchinson, J. The relation between crack growth resistance and fracture process parameters in elastic-plastic solids. *J. Mech. Phys. Solids*. **1992**, *40(6)*, 1377-1397. DOI: 10.1016/0022-5096(92)90020-3

[28] Kafkalidis, M.; Thouless, M. The effects of geometry and material properties on the fracture of single lap-shear joints. *Int. J. Solids Struct*. **2002**, *39(17)*, 4367-4383. DOI: 10.1016/S0020-7683(02)00344-X

[29] May, M.; Hesebeck, O.; Marzi, S.; Böhme, W.; Lienhard, J.; Kilchert, S.; Brede, M.; Hiermaier, S. Rate dependent behavior of crash-optimized adhesives–Experimental characterization, model development, and simulation. *Eng. Fract. Mech*. **2015**, *133*, 112-137. DOI: 10.1016/j.engfracmech.2014.11.006

[30] Hesebeck, O.; Meyer, U.; Sondag, A.; Brede, M. Investigations on the energy balance in TDCB tests. *Int. J. Adhes. Adhes*. **2016**, *67*, 94-102. DOI: 10.1016/j.ijadhadh.2015.12.031

[31] Blackman, B.; Hadavinia, H.; Kinloch, A.; Paraschi, M.; Williams, J. The calculation of adhesive fracture energies in mode I: revisiting the tapered double cantilever beam (TDCB) test. *Eng. Fract. Mech*. **2003**, *70(2)*, 233-248. DOI: 10.1016/S0013-7944(02)00031-0

[32] Karac, A.; Blackman, B.; Cooper, V.; Kinloch, A.; Sanchez, S.; Teo, W.; Ivankovic, A. Modelling the fracture behaviour of adhesively-bonded joints as a function of test rate. *Eng. Fract. Mech*. **2011**, *78(6)*, 973-989. DOI: 10.1016/j.engfracmech.2010.11.014

[33] Alvarez, D.; Blackman, B.; Guild, F.; Kinloch, A. Mode I fracture in adhesively-bonded joints: A mesh-size independent modelling approach using cohesive elements. *Eng. Fract. Mech*. **2014**, *115*, 73-95. DOI: 10.1016/j.engfracmech.2013.10.005

Table 1: Cohesive law parameters for each test and average

Test	Bond Line Length [mm]	Bond Line Thickness [mm]	Peak Force [N]	Initial Stiffness [MPa/mm]	Critical Energy Release Rate [kJ/m²]	Peak Traction [MPa]	Ratio of Plastic to Critical Energy Release Rate
Test 3	13.46	0.637	607.78	1604.24	2.387	39.83	0.1148
Test 5	13.52	0.697	624.96	1636.45	2.777	41.58	0.1069
Test 6	13.52	0.681	562.68	1379.51	2.820	35.58	0.1351
Test 7	12.67	0.604	550.87	1708.72	3.280	41.08	0.0853
Test 8	13.05	0.655	591.14	1362.23	3.590	41.14	0.1228
Test 9	12.51	0.730	511.14	1362.76	3.017	39.33	0.1451
Test 10	13.27	0.584	669.53	1402.15	3.437	46.70	0.1693
Test 11	13.72	0.586	618.25	1283.06	3.360	37.28	0.1410
Test 12	13.12	0.590	589.26	2298.77	2.826	37.21	0.1608
Average	13.20	0.640	591.73	1559.76	3.055	39.97	0.1312
Std. Dev.	0.38	0.051	43.63	295.88	0.366	3.07	0.0251

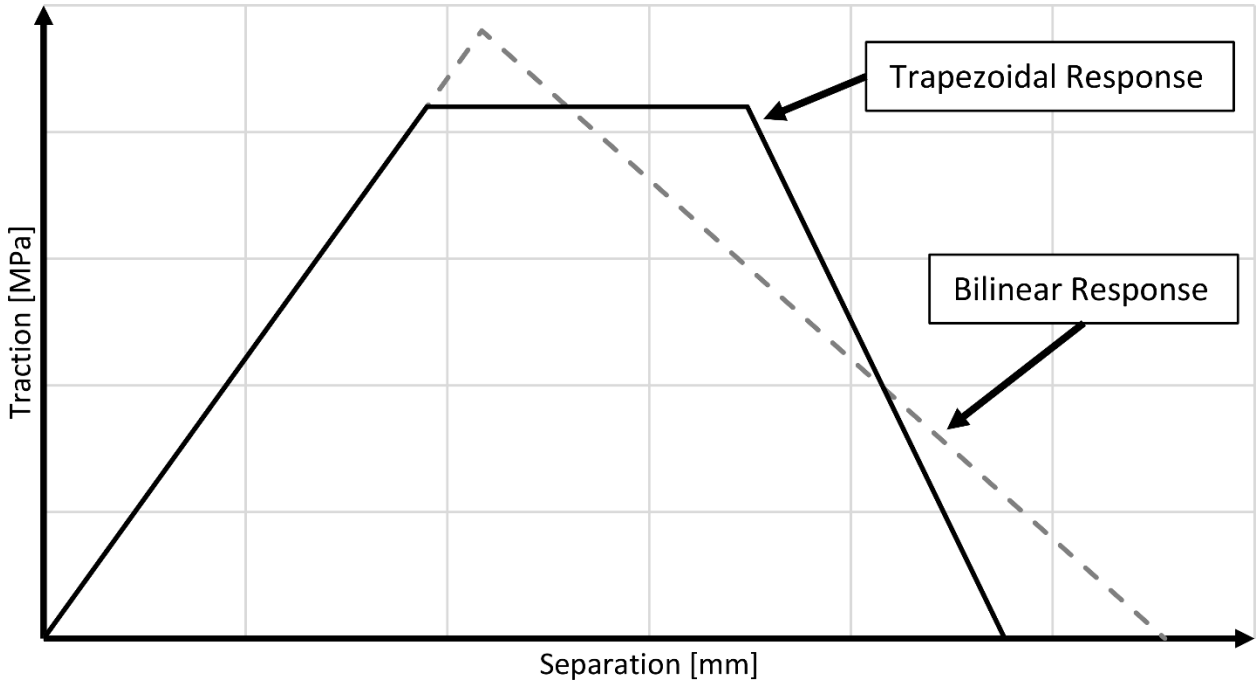

Figure 1: Typical cohesive traction–separation response

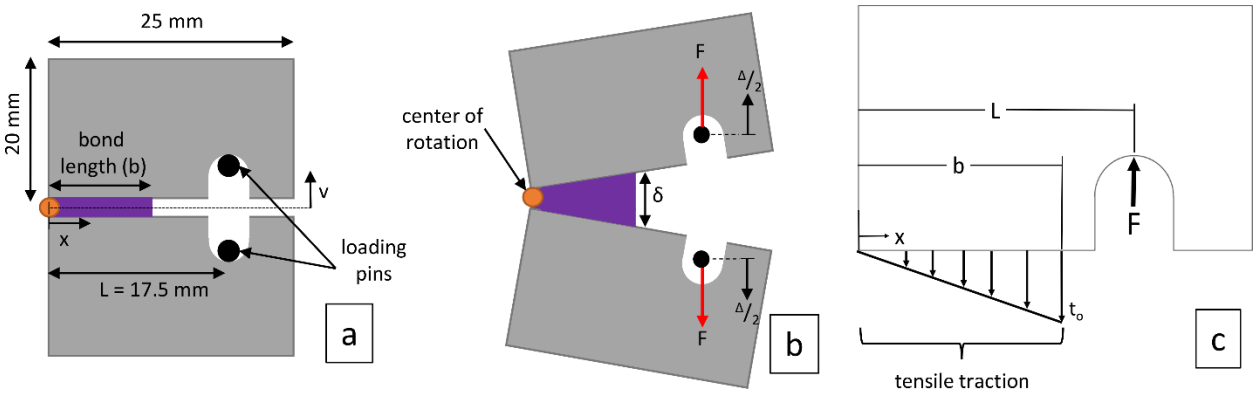

Figure 2: Important dimensions used in analysis (a), loading schematic (b) and free body diagram (c) developed by Dastjerdi

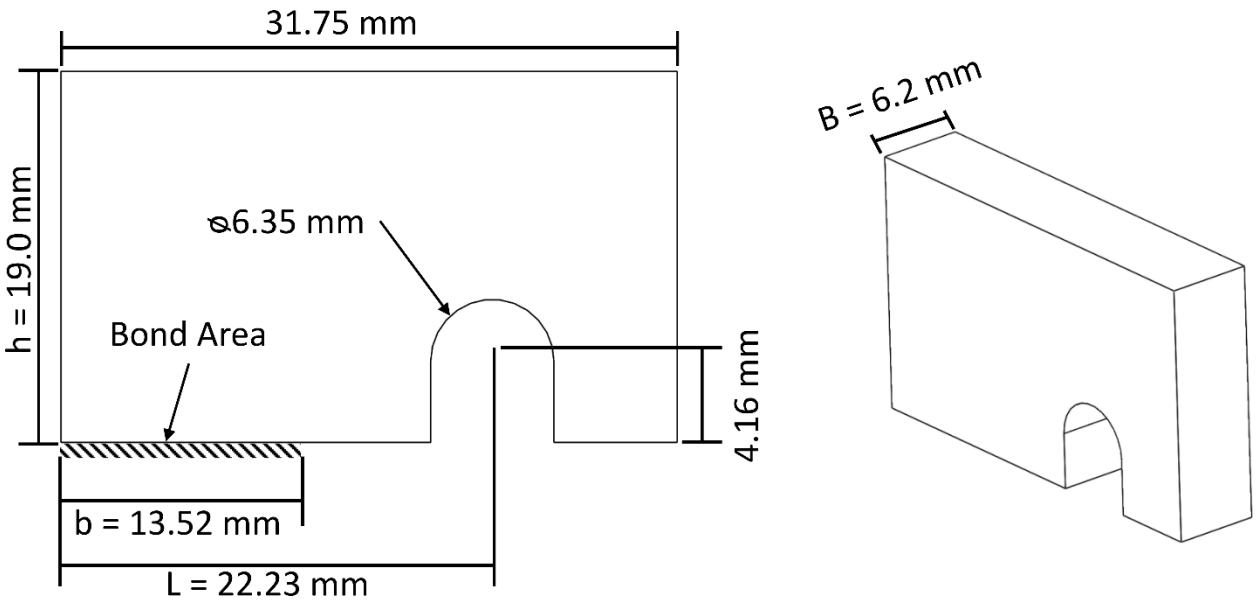

Figure 3: Dimensions of adherends used to create RDCB test samples

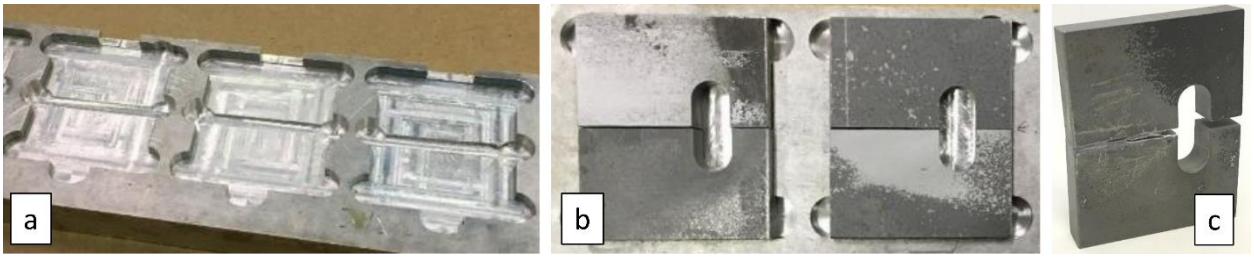

Figure 4: t sample bonding fixture (a); samples in place for curing (b); sample after testing (c)

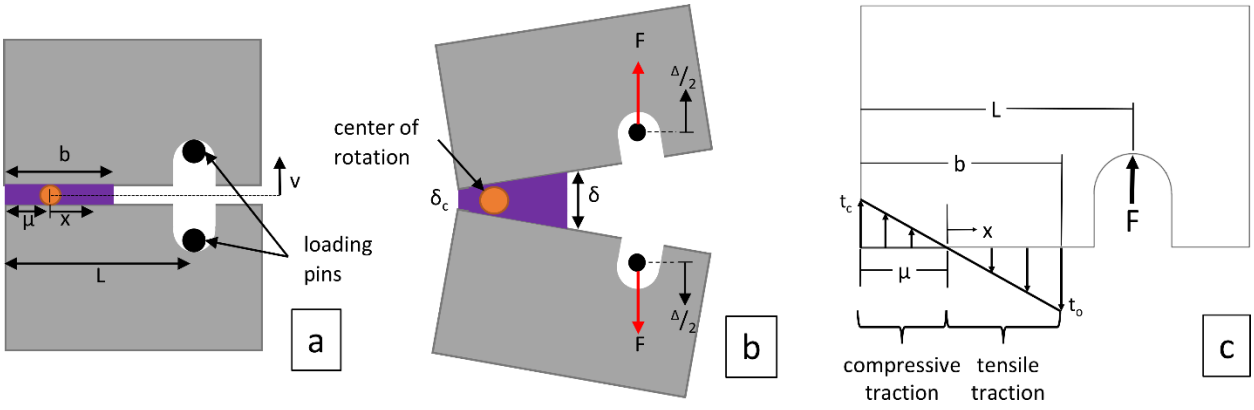

Figure 5: Important dimensions used in analysis (a), loading schematic (b) and updated free body diagram (c)

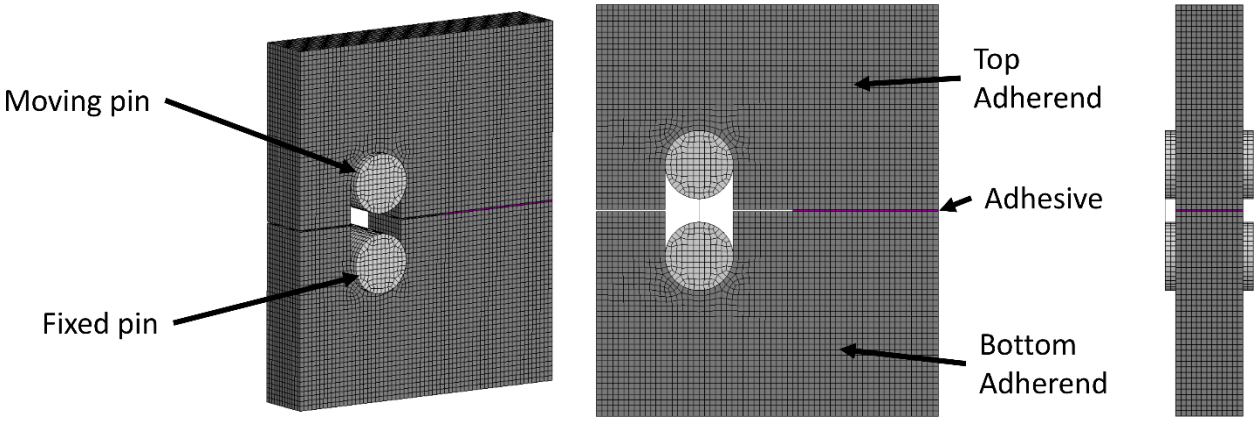

Figure 6: Deformable adherend finite element model

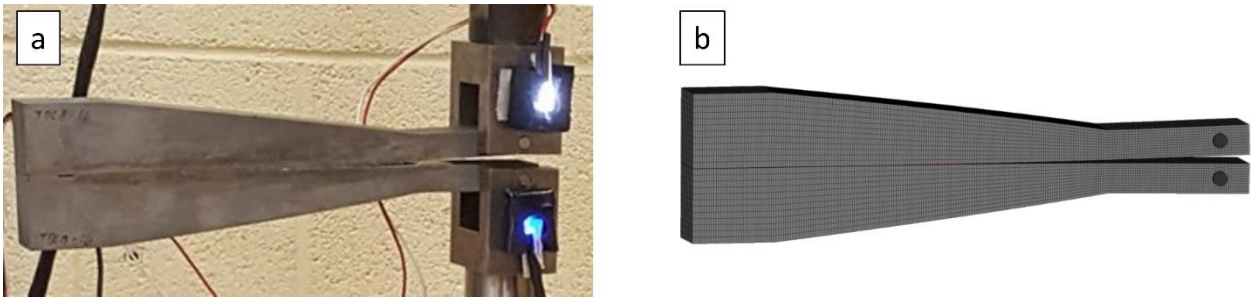

Figure 7: DCB test (a) and model (b)

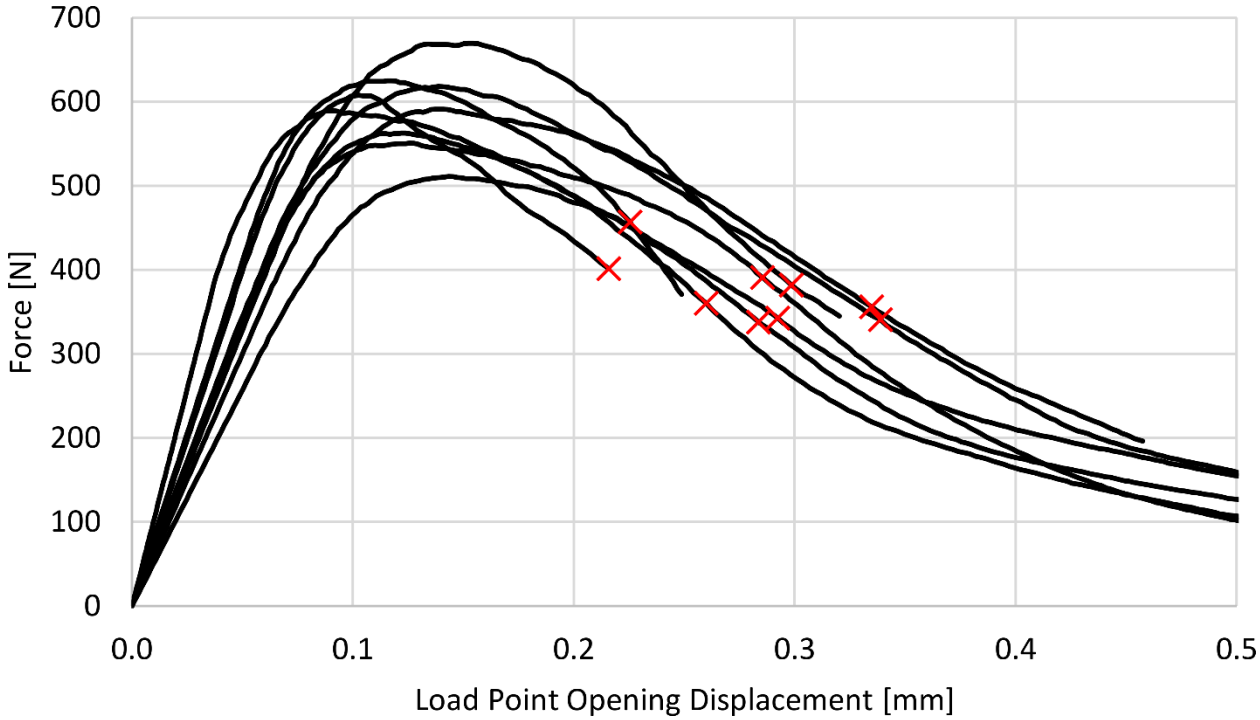

Figure 8: Force-load point opening displacement response of RDCB samples (n = 9)

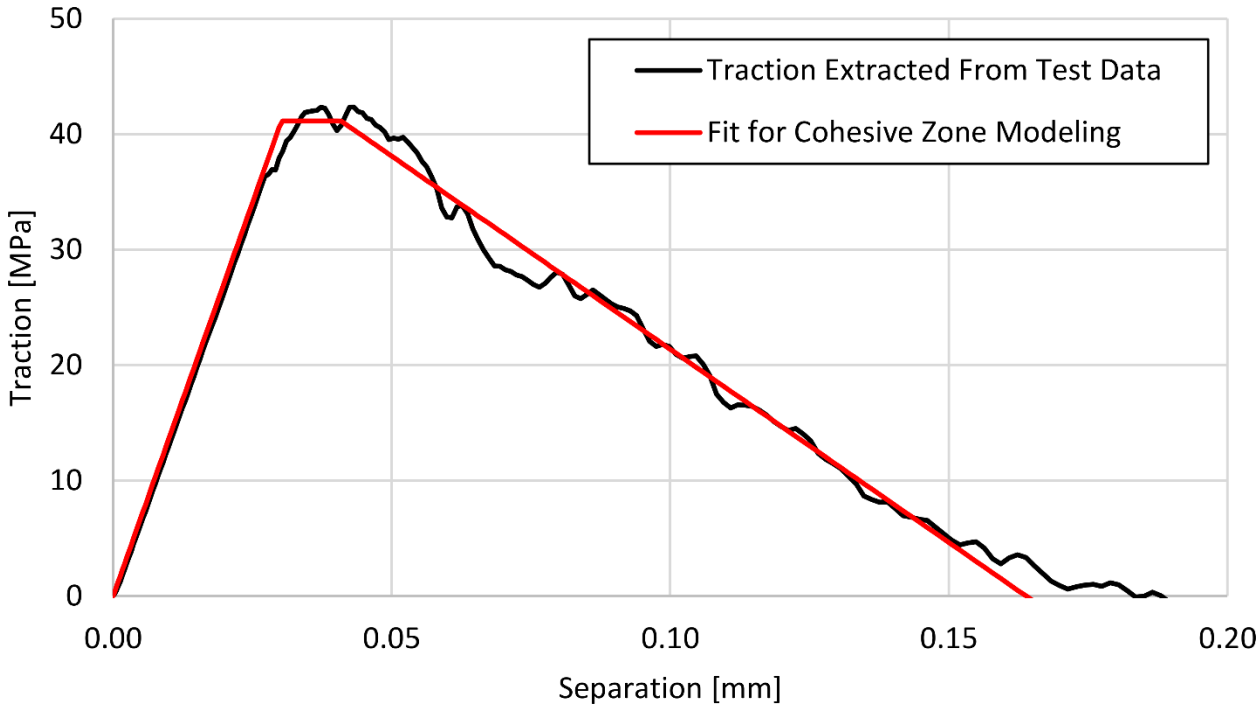

Figure 9: Fitting of trapezoidal cohesive law to test traction-separation

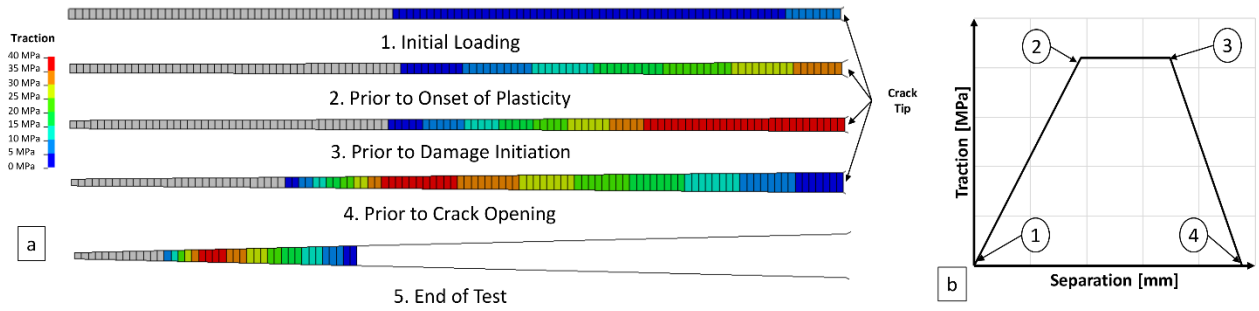

Figure 10: Progress of bond line stress states during loading (a) and corresponding traction at crack tip (b)

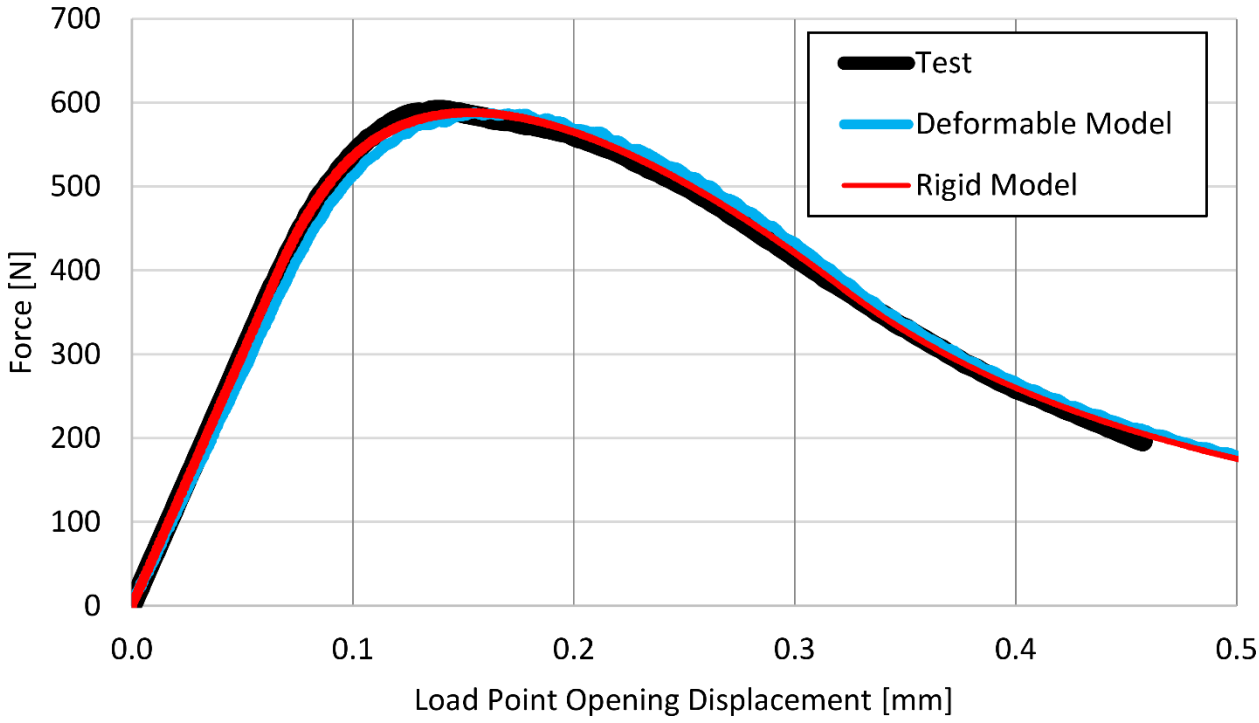

Figure 11: Comparison of test force-displacement to rigid and deformable models of Test 8

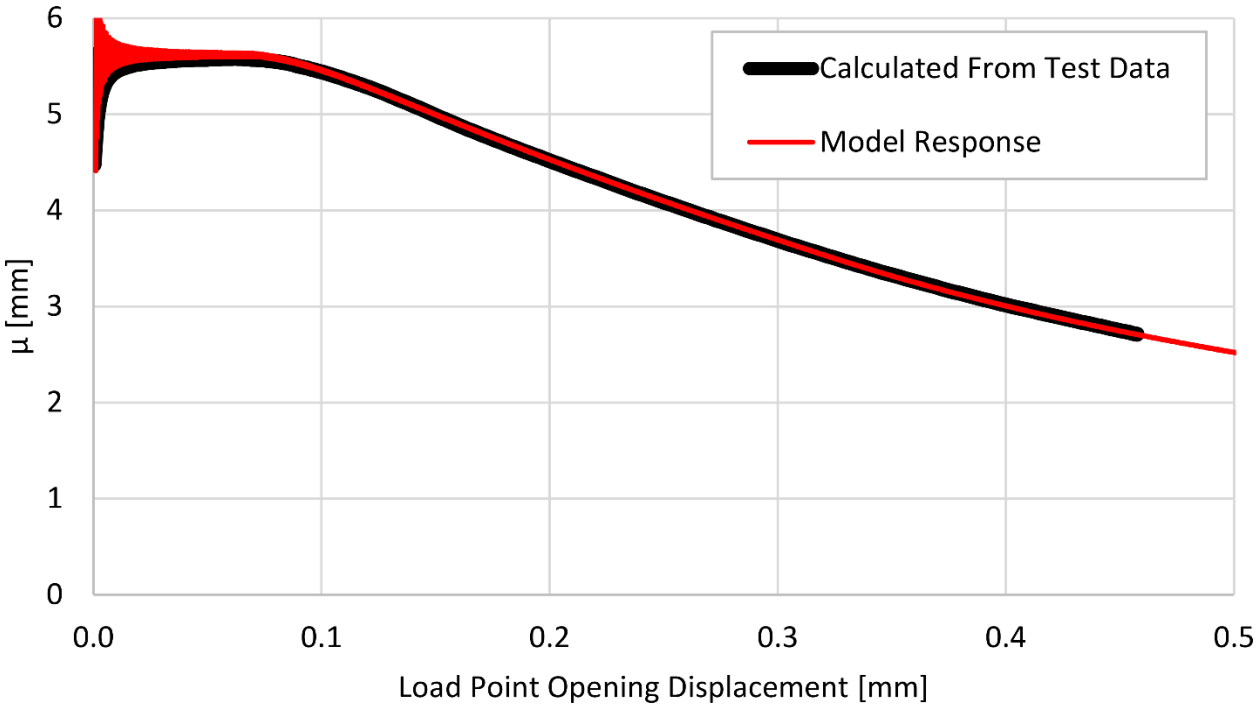

Figure 12: Shift in neutral axis calculated from test and rigid finite element model of Test 8

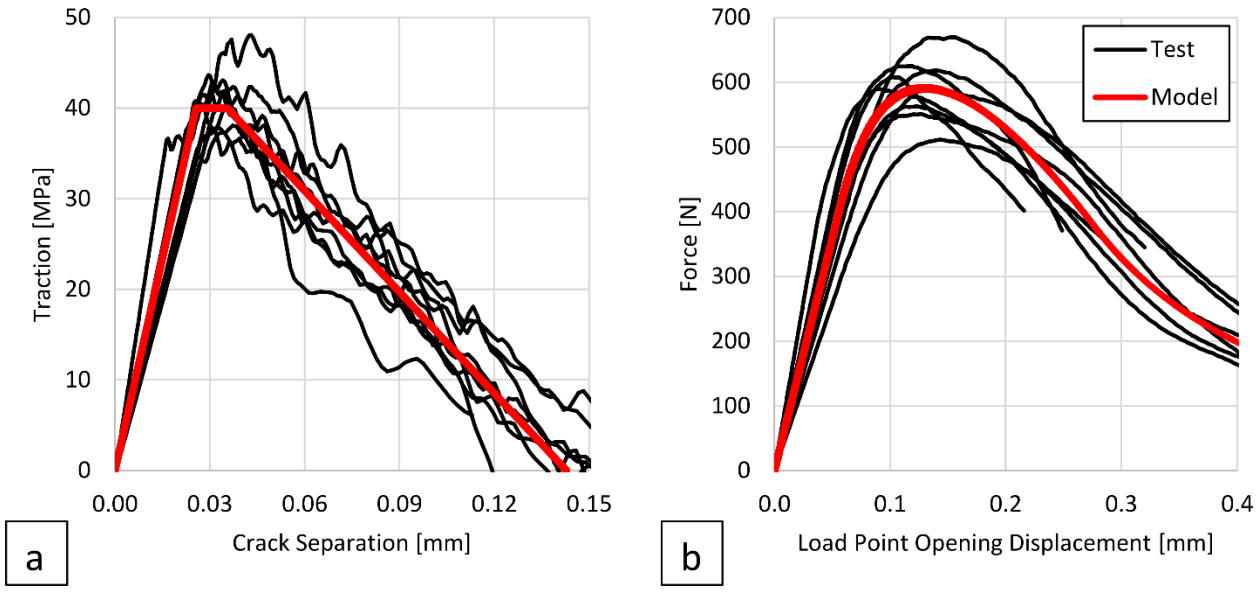

Figure 13: Calculated test traction-separation (a) and measured test force-load point opening displacement (b) compared to average model

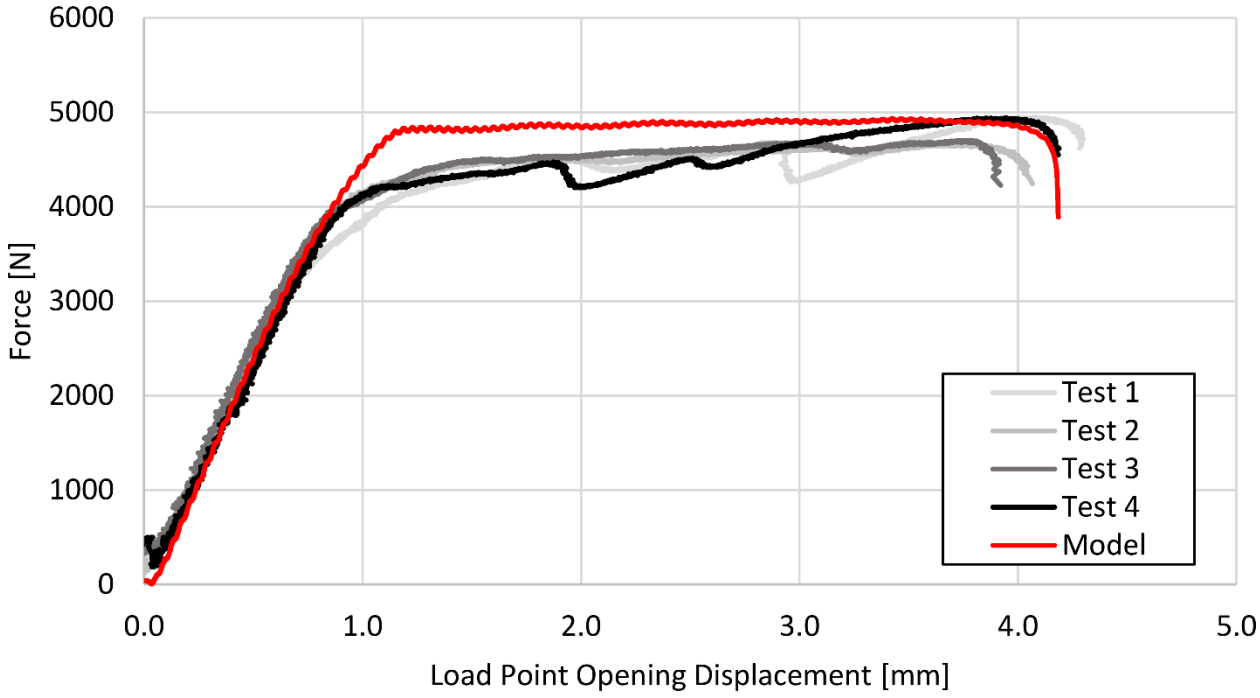

Figure 14: Comparison of TDCB tests and model response using RDCB derived cohesive material properties